Faraday Discussions

What stress components drive mechanochemistry? A study of ZDDP tribofilm formation

Journal:	*Faraday Discussions*
Manuscript ID	FD-ART-06-2022-000123.R1
Article Type:	Paper
Date Submitted by the Author:	26-Jul-2022
Complete List of Authors:	Fang, Lu; University of Pennsylvania School of Engineering and Applied Science, Mechanical Engineering & Applied Mechanics Korres, Spyridon; ExxonMobil Technology and Engineering Company, Lubricants Technology Lamberti, William; ExxonMobil Technology and Engineering Company, Materials and Catalysis Webster, Martin; University of Pennsylvania School of Engineering and Applied Science, Mechanical Engineering & Applied Mechanics Carpick, Robert; University of Pennsylvania School of Engineering and Applied Science, Mechanical Engineering & Applied Mechanics

What stress components drive mechanochemistry? A study of ZDDP tribofilm formation

Lu Fang[1]; Spyridon Korres[2]; William A. Lamberti[2]; Martin N. Webster[1]; Robert W. Carpick[1]

[1]Department of Mechanical Engineering & Applied Mechanics, University of Pennsylvania, Philadelphia, Pennsylvania 19104, United States
[2]ExxonMobil Research and Engineering Company, Lubricant Technology, Annandale, NJ, 08801, United States

KEYWORDS: Tribology, Mechanochemistry, antiwear additives, ZDDP, lubricants, tribofilm

Abstract

Zinc diakyldithiophosphate (ZDDP), the most widely used antiwear additive in engine oils, has been extensively studied over the last few decades to help understand the origin of its effectiveness. Glassy phosphate-based tribofilms, approximately 100 nm thick, are often formed on surfaces sliding in ZDDP-containing oils, which help to prevent or reduce wear. Recent studies reveal that a combination of applied shear and compressive stresses drive mechanochemical reactions that promote tribofilm growth, and that growth is further accelerated by increased temperature. While recent work has shown that compressive stress alone is insufficient to form tribofilms, the individual effects of the shear stress and compressive stresses are not fully understood. Here, shear and compressive stresses are studied separately by using different ratios of high-viscosity, high-traction fluids for testing. This allows the areal mean compressive and shear stresses in the fluid when confined at a loaded sliding interface to be independently controlled while driving tribofilm growth, which we refer to as stress-controlled mechanochemical reactor. Tribofilms derived from a secondary ZDDP were generated using a tungsten carbide/tungsten carbide ball-on-disk contact in the full elastohydrodynamic lubrication (EHL) regime using a mini-traction machine (MTM), meaning that solid-solid contact is avoided. The MTM was equipped with a spacer layer imaging (SLIM) capability, permitting *in situ* measurement of tribofilm thickness during its growth. The well-separated sliding surfaces generated by the high viscosity fluids confirm that solid-solid contact is not required for tribofilm formation. Under these full fluid film EHL conditions, shear stress and temperature promote tribofilm growth in accordance with stress-augmented thermal activation. In contrast, under constant shear stress and temperature, compressive stress has the opposite effect, inhibiting tribofilm growth. Using the extended Eyring model for shear- and hydrostatic pressure-affected reaction kinetics, an activation energy of 0.54 ± 0.04 eV is found, consistent with prior studies of ZDDP. The activation volume for shear stress is found to be 0.18 ± 0.06 nm^3, while that for compressive stress component is much smaller, at 0.010 ± 0.004 nm^3. This not only confirms prior work supporting that shear stress drives tribofilm growth, but demonstrates and quantifies how compressive stress inhibits growth, consistent with the rate-limiting step in tribofilm growth involving a bond-breaking reaction. Implications of these findings are discussed.

1. Introduction

Lubricants are used to improve energy efficiency and reduce material damage by minimizing friction and preventing wear within sliding and rolling contacts. Most modern lubricants contain antiwear additives to protect the rolling and sliding components from severe wear under boundary and mixed lubrication regimes (*i.e.*, the lubricant film thickness is not enough to separate the two surfaces). Zinc dialkyldithiophosphates (ZDDPs), initially developed as corrosion and oxidation inhibitors in 1941 (1), are now the most common family of anti-wear additives. The antiwear properties of ZDDPs were not discovered until 1955 (2), but due in part to the anti-wear performance and cost-effectiveness, and are used in almost all commercially available engine oils (3). The general molecular structure is shown in ***Figure 1*** (3).

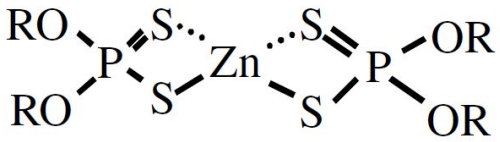

Figure 1. ZDDP molecular structure. Types of ZDDPs are differentiated by their radical groups (R-group) which are often primary alkyls, secondary alkyls, or aryl groups (3)

The lubrication condition in sliding or rolling lubricated contacts depends directly on the thickness of the lubricant confined between the surfaces. This thickness increases with increasing entrainment speed (mean speed of the two surfaces), increasing lubricant viscosity, and decreasing applied pressure, resulting in a transition from direct solid-solid contact (the boundary regime) to a full fluid film between the surfaces (the hydrodynamic regime or, in the case of conformal contacts under high load conditions, the elastohydrodynamic regime), with the mixed regime in between (4). Under mixed and boundary lubrication conditions, ZDDPs decompose and form a protective surface-bound layer, known as a tribofilm, at locations where the surfaces experience sliding contact. The tribofilm prevents severe wear of the underlying substrate, particularly for ferrous-based materials including steel, but also for other materials, such as silicon (5), metals, or metal alloys (6–9), ceramics (10–12), and diamondlike carbon (DLC) coatings (13,14). Many classes of additives form tribofilms; however, due to the widespread use of ZDDP and their crucial importance for wear protection, most studies have focused on ZDDP-derived tribofilms. The formation, composition, and structure of ZDDP-derived tribofilms have been studied for decades (3). ZDDP undergoes a series of chemical reactions to initially form isolated pad-like tribofilms on the substrate. The isolated pads then grow together to form a thin, rough, and patchy iron and zinc phosphate-containing glassy tribofilm which protects the underlying surfaces from wear (15). Studies of these tribofilms have revealed that the mechanical properties and structure are varied throughout the tribofilm, particularly with a substantial change in composition with depth. One earlier study by Bird and Galvin found that the tribofilms they studied consisted of polyphosphate in the uppermost layer, which gradually changed to orthophosphate and pyrophosphate near the substrate (16). A thin sulfur-rich layer exists beneath this thick phosphate tribofilm, which may assist in

bonding the tribofilm to the substrate (6,17). ZDDP tribofilms exhibit self-limiting tribofilm growth which results in tribofilms that typically are approximately 50-100 nm thick (18).

Although ZDDP-derived tribofilms have been studied substantively, the mechanisms driving its growth and properties are still not well understood. Investigating the driving forces that trigger the initiation and growth of the tribofilm is the key to unlocking a better understanding of ZDDP tribofilm formation. Establishing a better understanding of these processes will allow development of optimized anti-wear technologies in a broadening range of conditions. In particular, to protect vehicle emission systems, the levels of metals, P, and S are limited in fully formulated engine oils (19). Furthermore, changes in vehicle drive train configurations, including increasing use of electric vehicles (EVs), hybrid technologies, and alternate fuels, result in changes to the demands on and the operating environment for anti-wear additives (20,21). While studies have focused on ZDDP, the understanding of these mechanisms is potentially relevant to a broad range of antiwear, extreme pressure, and friction modifier additives. For example, the self-limiting growth of tribofilms derived from solid nanoparticles that provide anti-wear performance has been reported recently (22–25). Ultimately, knowledge of tribofilm initiation and growth will allow optimization of current additives in different applications and environments, and will help guide new additive technologies.

Recent attention has turned to study how mechanochemical mechanisms play a role in ZDDP tribofilm formation at the nano- (5,26), micro- (9,27), and macroscale (12,28). Several recent studies have focused on the specific role that applied stress has on tribofilm generation (5,9,12,26–28). Experimental studies include the use of in-situ bench-scale testing methods, such as single-asperity atomic force microscope (AFM) methods and mini-traction machines with spacer layer imaging (MTM-SLIM). Gosvami *et al.* were the first to explore the mechanochemical response of ZDDP by using AFM (5). In this study, they used a sharp amorphous carbon-coated AFM tip scanning over a nanoscale area on a pure iron substrate (with a native oxide) under different applied normal loads and temperatures in a commercial-grade synthetic hydrocarbon oil containing a standard commercial ZDDP package involving primary and secondary ZDDP molecules. The morphology of the rubbed area was periodically monitored using the AFM imaging mode, allowing tribofilm growth to be quantified over time. Compressive stress (based on the mean value estimated from Hertzian mechanics applied to the tip-substrate contact) and temperature were found to be the main driving forces of the ZDDP decomposition and antiwear tribofilm formation, although the authors noted that they could not discount the possibility that shear stress – intrinsic to the sliding contact and directly correlated with the applied compressive stress – was driving tribofilm growth. The tribofilm growth rate followed the SATA model (29). Using a secondary ZDDP molecule, and then an ashless DDP, another single-asperity study by Dorgham *et al.* (Si tip, steel substrate) also showed that the reaction kinetics followed the SATA model (26).

One way in which stress may play a role is by inducing different levels of cross-linking within a polyphosphate tribofilm. According to molecular dynamics simulations by Mosey *et al.* of a simplified phosphorous-based tribofilm precursor molecule, cross-linking of a polyphosphate tribofilm increases strongly with compressive stress once the stress exceeds a threshold value of 5 GPa (30–33)1/1/0001 12:00:00 AM. This may explain why ZDDP-derived tribofilms do not form well on softer Al-based alloys, since their low hardness compared to steel (750-920 HV vs. 170-190 HV (8)) will prevent contact stresses from reaching the threshold value. Consistent with this idea, Gosvami *et al.* observed using the AFM technique that initially no ZDDP-derived tribofilm forms, and substantial plastic deformation of the Al occurs (9). After sufficient plastic deformation, the tribofilm forms, attributed to work hardening of the Al and thus higher compressive stress of the contact, leading to stress-induced tribofilm formation. There could be also mechanochemically-activated processes that play a role. For example, Loehlé and Righi used *ab in initio* molecular dynamics (AIMD) simulations to study a simple organophosphorous molecule, trimethylphosphite (TMPi), that is known to form tribofilms in experiments (34). The AIMD results showed that TMPi, when compressed between sliding iron surfaces, reacts with the iron surfaces to form iron phosphide, and that the reaction rate is faster than that expected on a free surface. The difference is attributed to force-induced confinement. Collectively, these studies show that compressive stress can influence the growth rate as well as the chemical composition and the mechanical properties of the tribofilm.

Recently, Zhang, and Spikes used MTM-SLIM in an innovative way to provide even more evidence that the growth kinetics of tribofilm formation followed the SATA model (12). These experiments were conducted under full film elastohydrodynamic lubrication (EHL) conditions and demonstrated that surface-bound tribofilms can be formed in the absence of direct surface contact. The stress driving the growth comes from the compressive and shear stresses in the fluid acting on the precursor molecules, leading to tribofilm growth at the fluid-solid interface, instead of from the solid surfaces that confined the tribofilm precursor molecules and compress and shear them. The experiments were conducted under mixed rolling-sliding conditions using a high EHL traction fluid in order to attain high shear stresses. The work revealed that shear stress is required to drive tribofilm generation and subsequent growth. In a subsequent study, using the same technique, Spikes and coworkers showed that the ZDDP-derived tribofilm growth rate was found to be independent of ZDDP concentration in the solution, indicating the reaction follows zero-order kinetics (28).

A limitation of all of these previous studies is that it was not possible to independently control and vary the compressive stress and shear stress. In both sets of AFM experiments, the initial compressive stress (in the absence of the tribofilm) was used as the characteristic stress for model fitting. However, the elastic modulus of ZDDP tribofilms is much lower than the ferrous-based substrate (15-90 GPa (35) vs. 211 GPa (5)). Therefore, both the compressive and shear stress changed during the experiments as the tribofilm grows under the AFM probe; in fact, a reduction in these stresses as the tribofilm grows potentially explains the saturation of the tribofilm thickness. In addition, wear of the AFM probe can alter the compressive and shear

stresses in the contact. In Dorgham et al.'s study, the estimated radius of silicon AFM probes increased from an initial value of 15 nm to approximately 80 nm under an applied force of 150 nN. Even under no applied force (*i.e.*, only a small adhesive force acts), the probe radius increased to approximately 50 nm. Thus, the true stress state varies significantly over the course of the experiment, which is likely to impact tribofilm growth rates, although rate of change of tip radius reduces significantly as the experiment proceeds. Regardless, the lack of control of tip size, and lack of ability to independently vary shear and compressive stress, are key limitations of this approach.

In the MTM studies (12,28), the applied shear stress was controlled by altering the applied normal load. The shear stress generated within the EHL contact is determined by the high compression and shear properties of the lubricant used. For a single fluid, the shear stress generated in the contact region varies with temperature and compressive stress, preventing the independent variation of all three and thus making it challenging to determine their effects independently.

The goal of the present work is to determine the independent effects of compressive stress, shear stress, and temperature on tribofilm formation kinetics. The experiments were performed using the MTM-SLIM methodology previously developed by Zhang and Spikes (12), but modified to permit independent variation of shear and compressive stresses at chosen temperatures. Specifically, we used different combinations of lubricant base stocks to produce a series of blends with different EHL traction properties. These all contained the same amount of ZDDP, thus independently varying shear stress, compressive stress, and temperature without any alteration of chemically active species in the lubricant. To effectively eliminated the likelihood of direct surface contact, the fluid blends were chosen to have sufficiently high viscosity, thus sufficiently thick EHL films were generated, allowing independent study of the stress components driving ZDDP-derived tribofilm formation.

2. Materials and Test Methods

2.1 Lubricant samples

A total of 9 different lubricant blends were used in the study, each containing 99 wt% of basestocks and 1 wt% ZDDP. The basestocks contain different combinations of a high EHL-traction fluid, polyisobutene (PIB) and a low EHL-traction fluid, polyalphaolefin with a kinematic viscosity of 40 cSt at 100 °C (PAO40). The ZDDP was a commercially available secondary type ZDDP. The detailed information is provided in ***Supplementary Table 1***.

2.2 Test methods

The PCS Instruments MTM-SLIM™ (London, UK) was used to generate both traction data vs. time and concurrent periodic *in-situ* tribofilm thickness measurements throughout the duration of the test, as well as to determine traction curves. In addition, the final end-of-test film profile was measured using a 2-D surface profilometer, Tencor™ P-7 (Milpitas, CA) to verify the

accuracy of the SLIM measurements. The root-mean-square roughness of the ball and the disk was measured using a Zygo NewView™ 6300 (Middlefield, CT) white light interferometer. The central lubricant film thickness was measured by using PCS EHD2 rig™ (London, UK). A TESCAN S8000X (Kohoutovic, Czech Republic) FIB/SEM equipped with a Time-of-Flight Secondary Ion Mass Spectrometer (ToF-SIMS) was used to study the chemical composition of the tribofilm.

3. Results and Discussion

The fluid blends used in this study contain different combinations of lubricant basestocks of a high traction base fluid (polyisobutylene, PIB), and a low traction base fluid (polyalphaolefin, PAO). At a given compressive stress, *P,* and temperature, *T*, the shear stress, τ, will depend on the PAO/PIB ratio, thus allowing independent control of the compressive and shear stresses at each temperature by using different fluid mixtures. We call this the "stress-controlled mechanochemical reactor". The full information for each blend is given in the Supplementary Information, ***Table S1***. The compressive stress reported at each combination of lubricant composition and temperature is the calculated maximum Hertzian pressure, and the shear stress is obtained from the multiplication of the compressive stress and the traction coefficients measured based on the traction curves in ***Figure S3*** and ***Figure S4***. The experiments were conducted with a tungsten carbide ball and disk to perform experiments up to high stresses while avoiding plastic deformation. During the MTM experiment, the shear stress over time stays the stable as shown in ***Figure S8***. The properties of the specimens are provided in ***Table S2***. The specific lubricant film thickness, which indicates whether the surfaces are sufficiently separated to avoid solid-solid contact, is given by the ratio of central lubricant film thickness (estimated using the well-established EHL theory (4) to be at least 116.5 nm for all experiments) and the composite roughness of the solid surfaces (measured using white light interferometry to be 5.4 nm) (***Eqn. S3***) (4). This corresponds to a specific lubricant film thickness of 21.6 or greater, which indicates that there is, as desired, a large fluid separation between the ball and the disk. The growth rate of the ZDDP tribofilm was extracted from the initial 30 minutes of the 6-hour experiments since tribofilm saturation was observed to begin at that point or later. An initial nucleation period observed to last approximately 10 minutes was excluded from the analysis, as shown in ***Figure S10***, ***Figure S11*** and ***Figure S12***.

The morphology of the WC disk underlying the ZDDP tribofilm was observed after tribofilm removal with EDTA. White light interferometry (WLI) measurements with vertical resolution better than 1 nm reveal no observable wear of the WC; a representative example is shown in ***Figure 2***. This shows that consumption of substrate material is not needed to grow the tribofilm. This contrasts with the hard and soft acid-base (HSAB) reaction model for ZDDP tribofilm growth which posits that substantial generation of wear particles is required to form ZDDP tribofilms (36). In the case of ferrous surfaces, the acid-base reaction involves the exchange of the softer Lewis acid, Zn^{2+} from ZDDP molecules, with the harder Lewis acid, Fe^{3+}

from substrate-derived iron oxide wear particles, which prefers to interact with phosphates from the ZDDP which are harder Lewis bases. While such ion exchange will modify the tribofilm composition and properties, the results here show that robust ZDDP tribofilms can be formed without Fe or other significant wear debris generation.

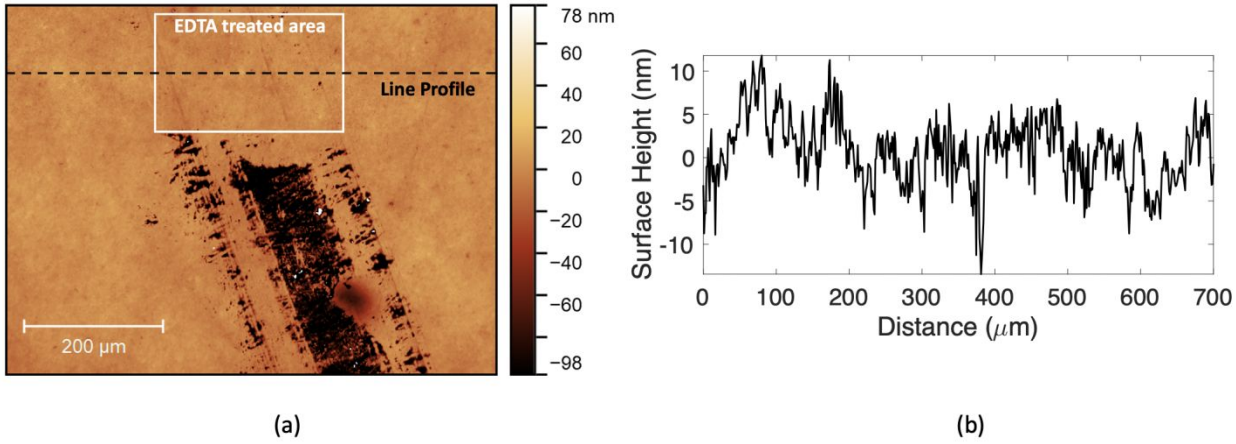

Figure 2. (a) White light interferometry (WLI) image of the running track on the WC disk after tribofilm removal with EDTA. The negative height measurement in the tribofilm area is an artifact due to the internal reflections within the transparent ZDDP tribofilm, as reported previously (37). (b) Line profile of the EDTA treated area of the WC disk, showing no observable wear.

Time-of-flight secondary ion mass spectrometry (ToF-SIMS) was used to investigate the composition of the ZDDP-derived tribofilms on the WC disk. The analytical conditions for SIMS analysis are shown in the supplementary document. Stevie *et al* demonstrate the TOF-SIMS instrument setup in (38). The positive and negative mass spectra comparison between the outer layer (approximately 1.7 nm) of the WC disk surface, which has been exposed to the ZDDP-containing blend during the MTM experiment, and the outer layer of the tribofilm are shown in ***Figure 3 (a)*** and ***(b)*** respectively. In the tribofilm area, there are several peaks attributed to hydrocarbon fragments ($C_2H_x^+$ and $C_3H_x^+$), and zinc-containing species (Zn^+, ZnO^+, $ZnOH^+$, ZnS^+ or ZnO_2^+, and Zn_2^+), while tungsten-containing peaks (W^+, WC^+, and WO^+) are absent, as expected. In addition, a large amount of O^- and a series of peaks attributed to phosphates (PO^-, PO_2^-, PO_3^-, and $P_2O_2H^-$) were found. Outside of the running track, a significant amount of WS^- was observed. This indicates that ZDDP reacts with the WC surface by either physisorption strong enough to remain after rinsing the sample, or forming a layer rich in W and S (e.g. tungsten sulfide, sulfate or mixed sulfides/oxides).

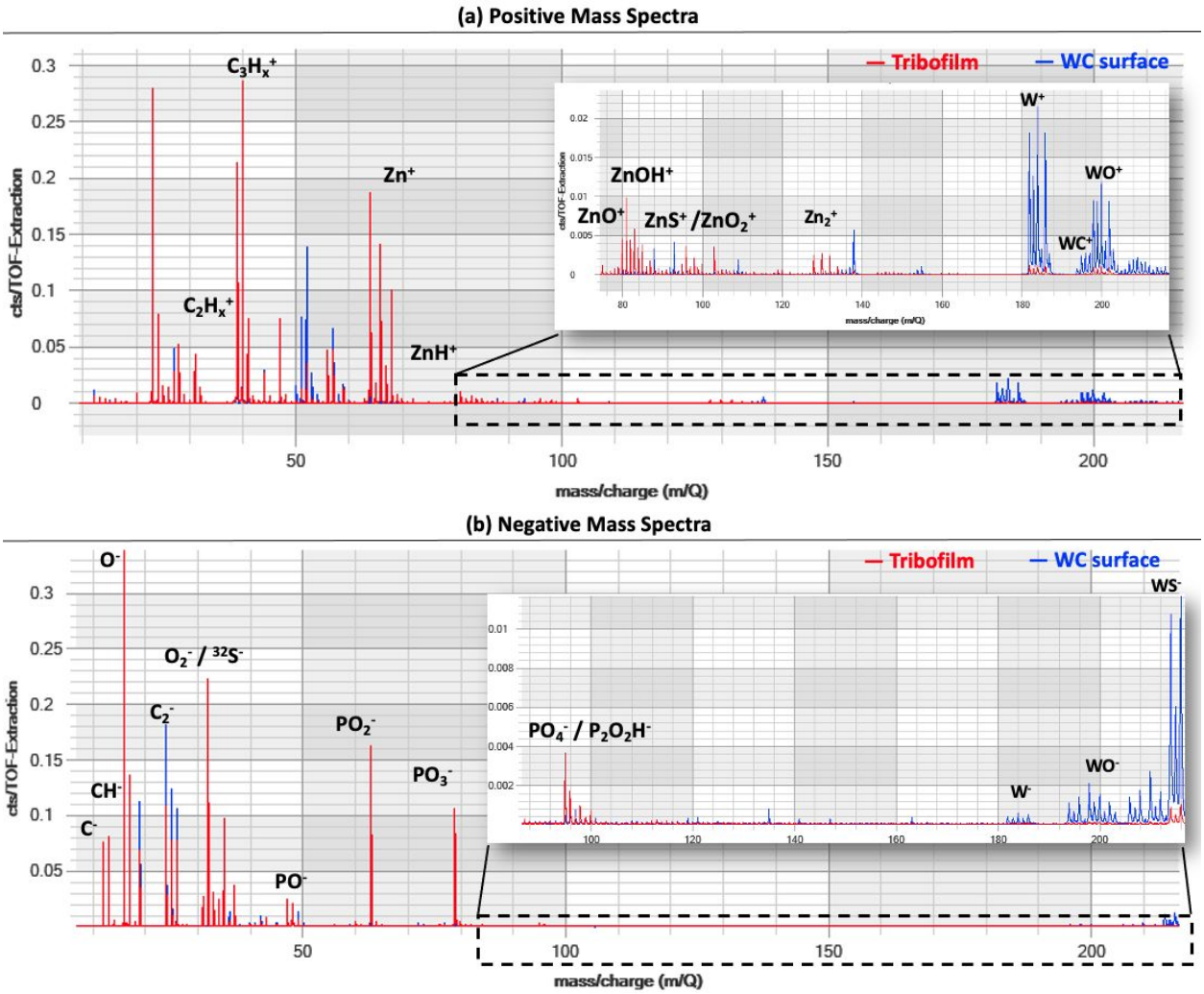

Figure 3. The (a) positive and (b) negative ion spectra comparison between the top layer (approximately 1.7 nm) of tribofilm and WC surface.

Figure 4 (a) is the ion-induced secondary electron image (iSEI) of a 400 x 400 μm^2 area, where the bright vertical stripe is the tribofilm that has grown in the running track, and the dark area is the WC substrate outside the running track. Corresponding secondary ion images of relevant elements are selected for ZDDP tribofilm chemical investigation. The element distribution maps of Zn^+ and W^+ in ***Figure 4(b)*** and ***(c)*** indicate that the tribofilm is mainly Zn^+ and lacks W^+. Less W^+ is incorporated into the tribofilm; the gradient in W^+ signal seen near the bottom of the tribofilm is most likely attributed to the ion beam mixing effect, where the primary ions can drive surface atoms ahead of the sputtering interface into the sample (39). Interface roughening can also arise as sputtering proceeds, resulting in loss of depth resolution during analysis. This result is consistent with the WLI result of ***Figure 2***, indicating that no wear of the WC substrate is involved in tribofilm growth. Nonetheless, some diffusional mixing at the original surface cannot be ruled out from this analysis alone. The intensity of $^{12}C_2^-$, shown in ***Figure 4(d)***, gets higher as milling approaches the WC surface. Since sulfur is difficult to identify as the difference in the mass number of $^{16}O_2^-$ and $^{32}S^-$ is subtle, the distribution of mass to charge ratio of 32 can be a combination effect from both $^{16}O_2^-$ and $^{32}S^-$. A second isotope of sulfur, $^{34}S^-$, was also chosen for analysis, and ***Figure 4(f)*** presents that sulfur is mostly observed in the top layer of

tribofilm. The element distribution maps of ***Figure 4(g) – (i)*** show that the tribofilm likely contains a significant amount of phosphate (PO^-, PO_2^-, PO_3^-). Therefore, the tribofilm is composed primarily of zinc and phosphate species, with enhanced S at the top surface, consistent with the typical composition of ZDDP-derived tribofilms found (3,17,40–43).

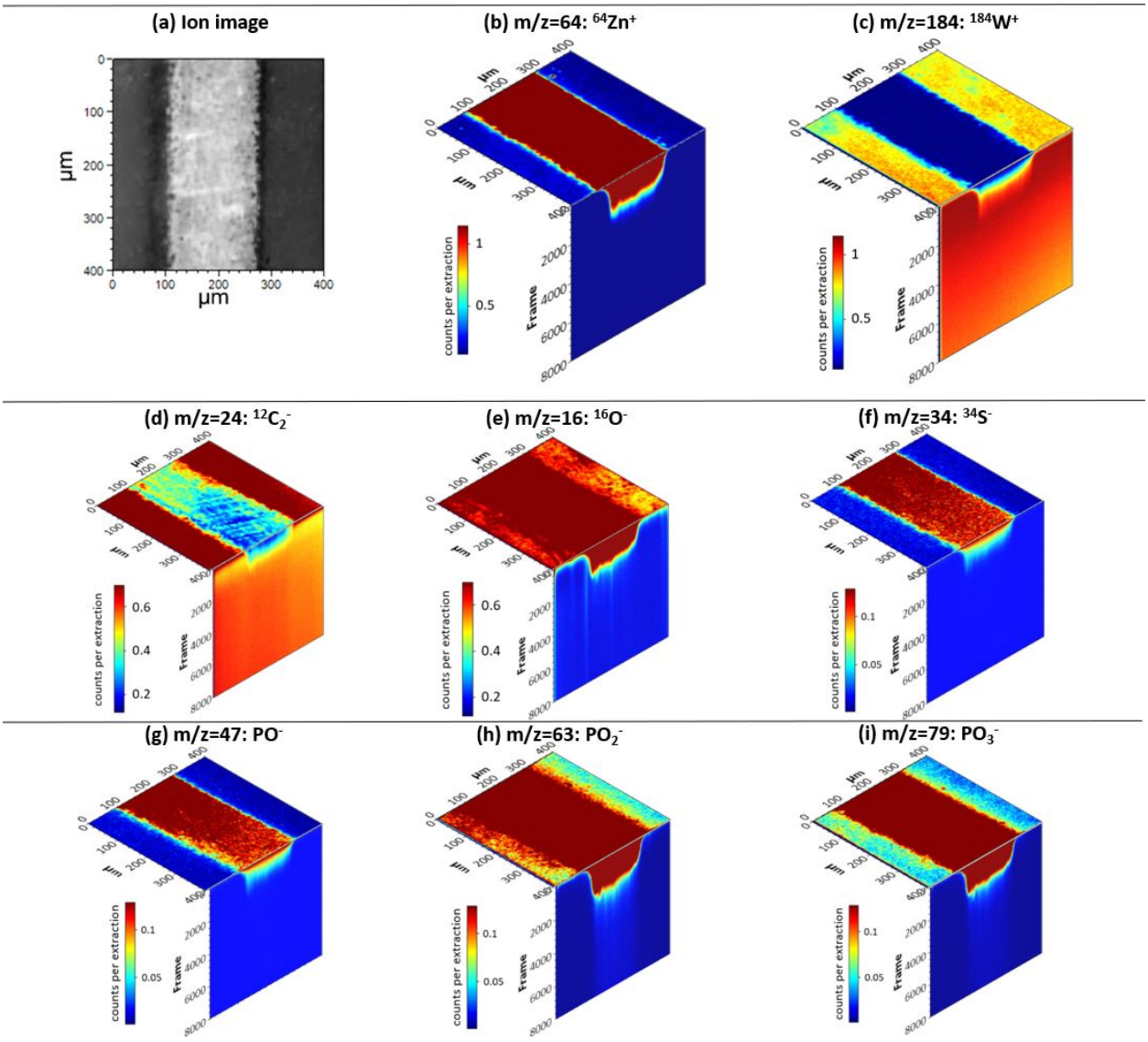

Figure 4. (a) Secondary ion image of the analyzed area, where the white region is the ZDDP-induced tribofilm, and the dark area is WC substrate. (b) and (c) are the 3D view of the $^{64}Zn^+$ and $^{184}W^+$ element distribution in the analyzed area respectively. The element distributions of (d) $^{12}C_2^-$, (e) $^{16}O^-$, (f) $^{34}S^-$, (g) PO^-, (h) PO_2^-, (i) PO_3^- in the analyzed area.

2.1 Effect of compressive stress

In the first set of experiments, we varied the blend composition and the normal load to quantify the growth of tribofilms as a function of the compressive stress, with a fixed shear

stress and temperature as shown in ***Table 1***. This was done for two different pairs of temperature and shear stress values. The results show that with temperature and shear stress held constant, increasing the compressive stress reduces the rate of tribofilm growth as shown in ***Figure 5***. This demonstrates for the first time that compressive stress inhibits ZDDP tribofilm growth.

Experiment Subset 1 (T = 140°C; τ = 194±2 MPa)		**Experiment Subset 2 (T = 120°C; τ = 207±2 MPa)**	
Fluid composition	Compressive stress (GPa)	Fluid composition	Compressive stress (GPa)
89%PIB + 10% PAO	2.2	99%PIB	2
84%PIB + 15% PAO	2.3	89%PIB + 10% PAO	2.2
79%PIB + 20% PAO	2.4	84%PIB + 15% PAO	2.3
74%PIB + 25% PAO	2.5	79%PIB + 20% PAO	2.4

Table 1. Summary of blend information and contact stress

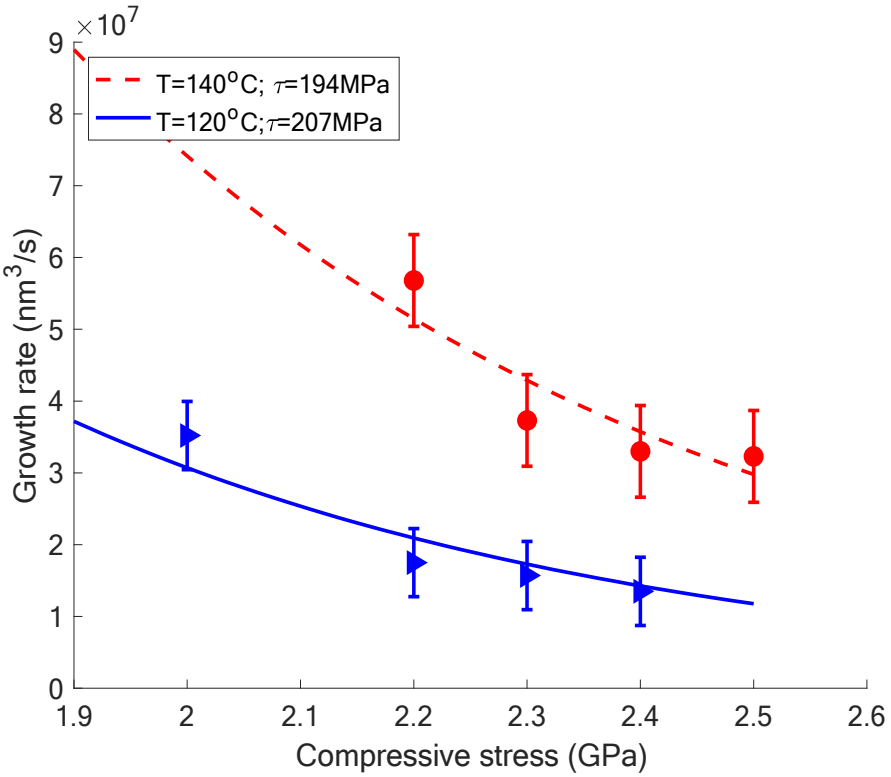

Figure 5. Dependence of tribofilm growth rate on the compressive stress. The legend indicates the values of temperature and applied shear stress used. The red dotted line and the blue solid line are fits of the extended Eyring model (Equation 3) at the respective temperatures and shear stresses.

2.2 Effect of Shear stress

In the second set of experiments, we explored the independent effect of shear stress on growth. Another series of different lubricant blends were formulated as shown in ***Table 2***. Two sets of experiments were performed at the same compressive stress of 2.5 GPa, but at two different temperatures, 100°C and 140°C.

Experiment Subset 1 ($T =$ 140°C; $P =$ 2.5 GPa)		**Experiment Subset 2 ($T =$ 100°C; $P =$ 2.5 GPa)**	
Fluid composition	Shear stress (MPa)	Fluid composition	Shear stress (MPa)
99%PIB	260	99%PIB	279
89%PIB + 10% PAO	234	89%PIB + 10% PAO	258
84%PIB + 15% PAO	218	79%PIB + 20% PAO	233
79%PIB + 20% PAO	207	64%PIB + 35% PAO	205
74%PIB + 25% PAO	196		

Table 2. Summary of blend information and shear stresses of two sets experiments

Figure 6 shows that the growth rate increases with applied shear stress, which confirms that the shear stress is a primary driving forces for growing the tribofilms as demonstrated by Zhang and Spikes (12,28).

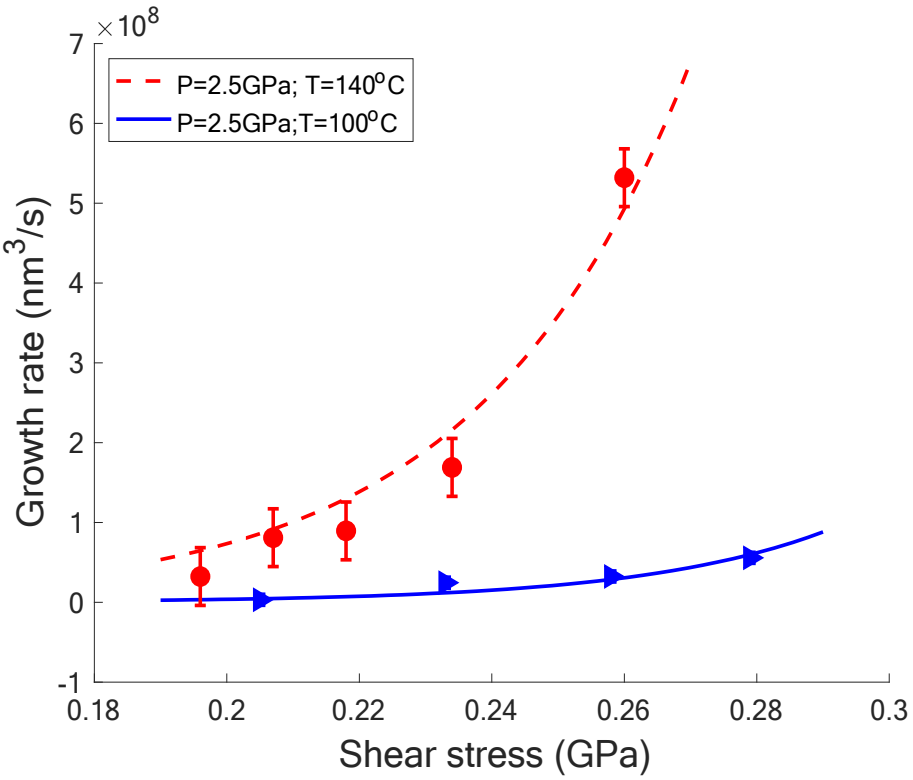

Figure 6. Dependence of tribofilm growth rate on the shear stress. The legend indicates the values of temperature and applied compressive stress used. The red dotted line and the blue solid line are fits of the extended Eyring model (Equation 3) at the respective temperatures and compressive stresses.

4.3 Effect of Temperature

In the third set of experiments, we studied the effect of temperature on tribofilm growth rate. Two subsets of experiments were performed, shown in ***Table 3***, with the compressive stress the same for both, and two different target shear stresses used since shear stress affects film growth strongly. For each subset of experiment, the target shear stress was approximately constant throughout the temperature range. To achieve the target shear stress, different blends were selected to run at each temperature and pressure condition. Set 1 was run at a compressive stress of 2.5 GPa and a shear stress of approximately 233 MPa. The other set was run under the same compressive stress but at a lower shear stress different shear stress of 207 MPa. The tribofilm growth rate was calculated with the same method as described previously.

Experiment Subset 1 ($P =$ 2.5 GPa; $\tau =$ 233±2 MPa)		**Experiment Subset 2 ($P =$ 2.5 GPa; $\tau =$ 207±2 MPa)**	
Fluid composition	Temperature (°C)	Fluid composition	Temperature (°C)
89%PIB + 10% PAO	140	79%PIB + 20% PAO	140
84%PIB + 15% PAO	120	74%PIB + 25% PAO	120
79%PIB + 20% PAO	100	64%PIB + 35% PAO	100
74%PIB + 25% PAO	80	54%PIB + 45% PAO	60

Table 3. Summary of blend information and applied temperature in Kelvin and Celsius of two sets of experiments.

The results shown in **Figure 7** illustrate that increased temperature also accelerates the tribofilm growth rate. Therefore, as seen consistently with all studies of ZDDP (3,5,12,28), tribofilm formation is thermally driven.

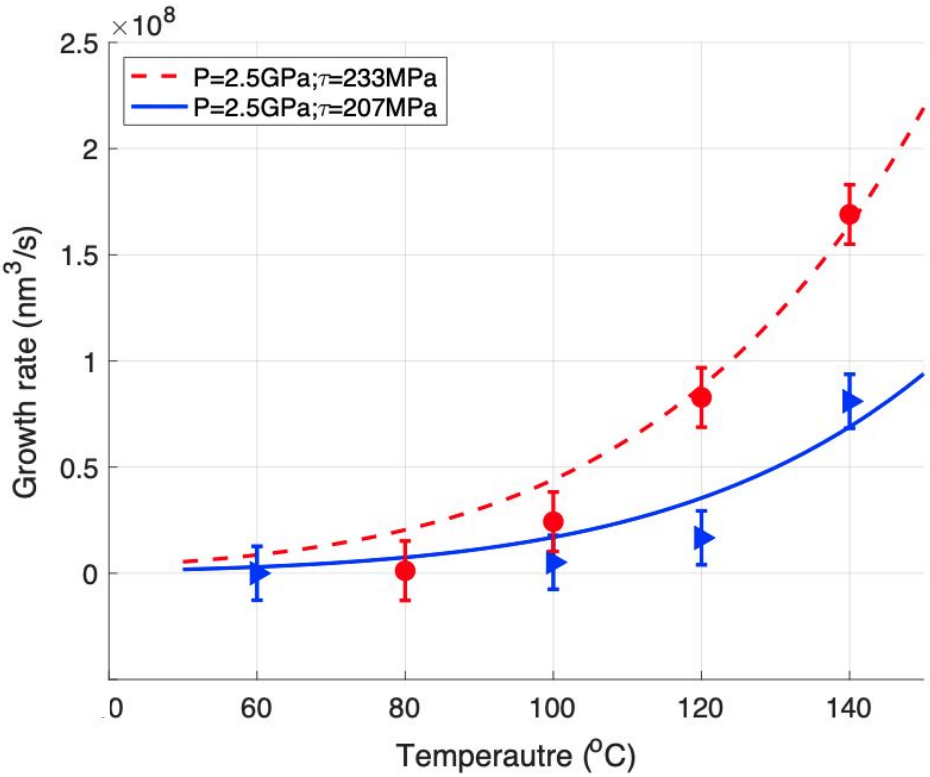

Figure 7. Dependence of tribofilm growth rate on the temperature. The legend indicates the values of applied compressive stress and shear stress used. The red dotted line and the blue solid line are fits of the extended Eyring model (Equation 3) at the respective temperatures and compressive stresses.

4.4 Extended Eyring model

The SATA model, which describes how activated processes including tribofilm growth are affected by stress, derives from multiple sources (29). One starting point is the model proposed by Bell (44) which is now widely used as the basis for mechanochemistry and tribochemistry (29), which proposed that the rate of force-assisted bond breakage can be determined by the following equation:

$$k = A\exp\left(-\frac{\Delta U_{act} - f\Delta x_{act}}{k_B T}\right) \quad (1)$$

where *k* is the rate constant, *A* is a pre-exponential factor, ΔU_{act} is the activation energy, is k_B Boltzmann's constant, and T is temperature. The force, f, applied to the system assists the forward reaction rate if it drives the system along the reaction coordinate (45). The reaction rate also determined by the activation length, Δx_{act}, which is defined as the difference in linear size of the reacting species in transition state vs. the initial state. To reduce the energy barrier, the work done on the system, $f\Delta x_{act}$, involves the component of the force along the direction of the chemical reaction process. If f is a driving force applied along the specific bond or on a molecule, the energy barrier will be reduced by $|f\Delta x|$. For example, a force that extends the length of a molecule will lower the activation barrier for a bond-breaking process. However, if f is an inhibitory force, the energy barrier will be increased, thus the work done to the system is negative, which is $-|f\Delta x|$. In practice, the applied force at the molecular level is complex to measure. However, it is feasible to estimate the applied stress during experiments, which corresponds to the average force applied per molecule assuming a uniform areal density of molecules. Thus, instead of activation length, one uses the activation volume. In this case, the rate constant is given by using the following equation (29):

$$k = A\exp\left(-\frac{\Delta U_{act} - \sigma\Delta V_{act}}{k_B T}\right) \quad (2)$$

where σ is the applied stress, and ΔV_{act} is the activation volume. ΔV_{act} is the difference in volume between the transition state (V_{TS}) and the initial equilibrium state or the reactant (V_R) (46). A positive activation volume indicates the volume of the transition state is larger, which would be the case for a bond breaking reaction. In contrast, a negative activation volume indicates the volume of the transition state is smaller, which indicates the applied stress is helping with bond formation.

The importance of the hydrostatic and the shear components of stress driving activated processes was considered by Ward in 1971, who was studying the temperature and shear rate dependence of the yield of polymers with applied tension and compression (47). He introduced an extended form of the Eyring model that considered the effect of both the compressive stress and the shear stress as follows:

$$k = A\exp\left(-\frac{\Delta U_{act} - \tau\Delta V_{act} + P\Delta\Omega_{act}}{k_B T}\right) \quad (3)$$

where ΔV_{act} is the activation energy corresponding to the shear stress, τ, and $\Delta \Omega_{act}$ is the activation energy corresponding to the compressive stress, P (the equation has been adapted from Ward to represent a growth rate, as opposed to a shear rate). With applied shear stress, a tension force can act on molecules that are constrained at their ends, which can promote bonds breakage. If a bond-breaking reaction is the rate-limiting step in tribofilm growth, then shear is expected increase the tribofilm formation rate and indeed the term $-\tau \Delta V_{act}$ inside the exponential will do just that. On the other hand, compressive stress will inhibit bond stretching and breaking. Thus, again if a bond-breaking reaction is the rate-limiting step in tribofilm growth, the activation barrier will increase. The term $P\Delta\Omega_{act}$ inside the exponential will also have that effect, where a positive value of *P* is used for the case of applied compressive stress. Such bond-breaking interactions could involve cleavage of sulfur and zinc bonds, or between sulfur and alkyl groups, and are discussed further below.

Since the tribofilm volume increases approximately linearly with time, it can be modeled a zeroth-order reaction, which was confirmed in MTM experiments by Zhang *et al. (28)*. Therefore, the growth rate of the tribofilm, Γ, can be modeled as the following:

$$\Gamma = \Gamma_0 \exp\left(-\frac{\Delta U_{act} - \tau \Delta V_{act} + P\Delta\Omega_{act}}{k_B T}\right) \quad (4)$$

where Γ_0 is defined as:

$$\Gamma_0 = V_m \nu \quad (5)$$

where the molar volume, V_m, was assumed to be 1 nm^3 in the ZDDP tribofilm, and the attempt frequency, ν. We obtained high-quality fits by using the values of parameters in ***Table 4*** to fit data sets in ***Figure 4***, ***5***, and ***6***.

	Experiment	Γ_0	ΔU_{act}	ΔV_{act}	$\Delta\Omega_{act}$
Compressive stress	Subset 1	1.10 x 10^{13}	0.54 eV	0.18 nm^3	0.01 nm^3
	Subset 2	2.16 x 10^{13}			
Shear stress	Subset 1	1.00 x 10^{13}			
	Subset 2	4.40 x 10^{13}			
Temperature	Subset 1	3.31 x 10^{13}			
	Subset 2	3.45 x 10^{13}			

Table 4. The prefactor, Γ_0, activation energy, ΔU_{act}, activation volume for shear stress, ΔV_{act}, and activation volume for compressive stress, $\Delta\Omega_{act}$, obtained from fittings of six different experiments.

The positive activation volumes found with two different components of stresses indicate a bond breaking reaction is the rate limiting step for tribofilm formation. The value of the activation energy estimated here is similar to ones found for ZDDP tribofilms grown on ferrous-based surfaces, which are between 0.58 to 1 eV as measured by both AFM (5) and MTM

(12,28) studies. This comparable value may indicate that any chemical reactivity differences between ferrous and WC-based surfaces for tribofilm growth is not dominant. Our energy barrier being on the lower end of the published range is consistent with our use of a secondary ZDDP; secondary ZDDP's grow tribofilms faster than primary ZDDP's and this may be due to a lower activation barrier, although the faster growth may also result from different attempt frequencies and activation volumes as suggested by Zhang *et al. (28),* and may be sensitive to the specific alkyl structures in the ZDDP molecules. Regardless, the large value of the activation volume for shear stress found here indicates that shear stress is very effective in driving tribofilm formation, while compressive stress is only modestly effective at inhibiting it.

There are multiple possible hypotheses for why compressive stress inhibits tribofilm formation. First, the increased compressive stress forces atoms to be closer to each other, which on the one hand can inhibit the bond stretching needed to assist with bond-breaking chemical reactions, while on the other hand, it can promote bond-formation reactions by confinement (keeping reactants in close proximity) and strain (modifying the energy landscape in a way that promotes bond formation).

Second, compression may inhibit bond breaking reactions needed to instigate adsorption of ZDDP precursor molecules on the sliding surface. Such adsorption is critical as the first step for ZDDP-derived tribofilm formation. Yamaguchi *et al.* showed that ZDDP initially adsorbed on the substrate through the sulfur atom of the P=S bond by inelastic electron tunneling spectroscopy (IETS) (48). This agrees with a later study by Ivanov *et al.*, who found the covalent linkages formation between the dithiophsophate groups and the substrate by ^{31}P proton nuclear magnetic resonance (NMR) spectroscopy (49). This is significant as such linkages are likely to be an important prerequisite to initiate tribofilm growth. Therefore, with shear stress, the S—Zn bonds can be easily stretched or broken, which can promote the oxidation and reduction reaction between the ZDDP molecule and the sliding surface to form tribofilm. Compressive stress likely inhibits breaking of the S—Zn bonds, which slows down the adsorption process, and thus the tribofilm growth is inhibited.

Third, compression may inhibit a key step identified in phosphate formation from ZDDP precursors. Jones *et al.* showed that the exchange between oxygen and sulfur atoms (O/S exchange) followed by the bond breakage between sulfur atom and the alkyl group is a well-known property of organic thiophosphates (50). Since the growth rate of secondary alkyl ZDDPs-derived tribofilm is much faster than other types of ZDDPs, the rupture of the O/S — R bonds could be the rate-determining step of tribofilm formation (28). After the adsorption of the precursor molecules, the bond cleavage of O/S — R is more likely caused by shear stress instead of compressive stress, thus the tribofilm formation rate reduces when increasing the compressive stress.

Fourth, when the surface is subjected to high compressive stress, the pressure-viscosity effect will result in dramatically higher viscosity fluid within the contact (51). Compressive stress enhances intermolecular forces which will enhance viscosity, and further can affect the conformation of the lubricant molecules, changing the lubricant's viscous behavior locally (52,53). This higher viscosity will lead to lower molecular mobility, which to first order will change according to Stokes-Einstein equation:

$$D = \frac{k_B T}{6\pi r \eta} \quad (6)$$

where D is the Brownian diffusivity, and r is the radius of molecule. Thus, the diffusivity varies inversely with the viscosity. Therefore, with the pressure-induced high local viscosity, it reduces the mobility of the ZDDP, which may constrain its ability adsorb on the surface. Thus, the reaction rate is reduced.

As mentioned above, mechanisms by which compression should promote tribofilm growth have been identified, namely compression-induced cross-linking of the phosphate network (30–33)1/1/0001 12:00:00 AM, and compression-induced reaction with the substrate (34). The present results do not rule out that these mechanisms occur and are consequential for tribofilm growth and properties. However, the results do strongly indicate that such mechanisms are not rate limiting steps that control the tribofilm growth rate; rather, a bond-breaking mechanism, inhibited by compression and promoted by shear, is the controlling reaction.

4. Conclusions

We developed stress-controlled mechanochemical reactor, which enabled study of the independent effects of compressive stress, shear stress, and temperature on the mechanochemically-driven growth of tribofilms. The methodology incorporated the novel approach of Zhang and Spikes (12), where MTM experiments used a combination of high and low traction fluids, resulting in growth experiments under fully EHL conditions where no direct solid-solid contact occurs. Thus, all growth occurred due to forces solely transmitted through the lubricant film for which the contact conditions and stresses are well-characterized, avoiding convoluting effects from other factors such as substrate, asperity contact, changes in applied stresses as the tribofilm grows. Our adaptation was to vary the fluid composition for each experiment so that one stress component (either shear or compression) can be held constant while the other is varied; or both held constant as the temperature is varied. The methodology was applied to a pure secondary ZDDP dissolved in the fluid blends, from which the following results were obtained:

1. The extended Erying model (47), a SATA-based approach, describes the growth behavior of ZDDP-derived tribofilms well. We find an activation barrier of $\Delta U_{act} = 0.54 \pm 0.04\ eV$, an activation volume for shear stress of $\Delta V_{act} = 0.18 \pm 0.06\ nm^3$, and an activation volume for compressive stress of $\Delta\Omega_{act} = 0.010 \pm 0.004\ \ nm^3$;
2. The positive activation volumes for both shear stress and compressive stress indicate that a bond breaking reaction is the driving force for ZDDP tribofilm formation, instead of bond formation.
3. The reduction in ZDDP-derived tribofilm growth with increased compressive stress, while a mild effect (the activation volume is 18 times smaller in magnitude than that for

shear stress), indicates that the rate-limiting step in the series of reactions involved is one related to bond breaking, not bond formation or some other compressive-stress driven process.

4. Temperature and shear stress are each found independently to be strong factors driving ZDDP-derived tribofilm growth in accordance with prior work, but here demonstrated in the case of constant compressive stress.
5. The calculated activation energies from our work compare well with previous studies using ferrous surfaces, indicating similar reaction mechanisms.
6. The absence of wear in this study shows that cation exchange of the Zn with substrate ions, as proposed in the HSAB growth model (30–33), is not required for tribofilm growth. Incorporation of substrate ions, notably Fe in the case of ferrous substrates, is well-documented (54,55) and certainly affects tribofilm initiation, growth, and properties. It is thus important to consider for understanding ZDDP growth on ferrous substrates and other substrate materials that can participate in cation exchange reactions. However, the results here add to the body of work showing that ZDDP can forms solid, surface-bound tribofilms with self-limited growth driven by stress-augmented thermal activation, in the absence of any cation exchange.

The ability to study different composition of high-viscous high-traction fluids in the EHL regime provides unique insights, particularly the separation of normal and shear stress contributions to film growth. This enables a better understanding of the mechanochemical reactions for ZDDP-derived tribofilm formation. This approach can be beneficial for investigating the mechanisms of other reactive, film-forming additives for next-generation lubricant development.

5. Acknowledgment

R.W.C. and L.F. acknowledge support from NSF grants CMMI-1728360 and CHE-2023644. We thank A.R. Konicek, D. Eichelsdoerfer, B. Gooding, A. Jaishankar, N.N. Gosvami, H, Khare, and A. Schilowitz for useful discussions. We thank J. Ford for assistance with the ToF-SIMS measurements. This work was carried out in part at the Singh Center for Nanotechnology, which is supported by the NSF National Nanotechnology Coordinated Infrastructure Program under grant NNCI-2025608.

6. References

1. Asseff PA. Lubricant. United States Patent Office; 2,261,047, 1941.
2. Bidwell JB, Vermaire P. Lifters and Lubricants. SAE International. 1955;63:211–26.

3. Spikes H. The History and Mechanisms of ZDDP. Tribology Letters. 2004 Oct;17(3):469–89.

4. Stachowiak GW, Batchelor AW. Elastohydrodynamic Lubrication. In: Engineering Tribology. Elsevier; 2014. p. 293–370.

5. Gosvami NN, Bares JA, Mangolini F, Konicek AR, Yablon DG, Carpick RW. Mechanisms of antiwear tribofilm growth revealed in situ by single-asperity sliding contacts. Science. 2015 Apr 3;348(6230):102–6.

6. Barcroft FT, Bird RJ, Hutton JF, Park D. The mechanism of action of zinc thiophosphates as extreme pressure agents. Wear. 1982 Apr;77(3):355–84.

7. Suominen Fuller ML, De Jong KL, Kasrai M, Bancroft GM. Electroless Generation of Phosphate Films on Metals from Zinc Dialkyldithiophosphates. Chem Mater. 2000 May 1;12(5):1300–4.

8. Shimizu Y, Spikes HA. The Influence of Aluminium–Silicon Alloy on ZDDP Tribofilm Formation on the Counter-Surface. Tribol Lett. 2017 Dec;65(4):137.

9. Gosvami NN, Lahouij I, Ma J, Carpick RW. Nanoscale in situ study of ZDDP tribofilm growth at aluminum-based interfaces using atomic force microscopy. Tribology International. 2020 Mar;143:106075.

10. Haque T, Morina A, Neville A, Kapadia R, Arrowsmith S. Non-ferrous coating/lubricant interactions in tribological contacts: Assessment of tribofilms. Tribology International. 2007 Oct;40(10–12):1603–12.

11. Ueda M, Kadiric A, Spikes H. ZDDP Tribofilm Formation on Non-Ferrous Surfaces. Tribology Online. 2020 Oct 15;15(5):318–31.

12. Zhang J, Spikes H. On the Mechanism of ZDDP Antiwear Film Formation. Tribol Lett. 2016 Aug;63(2):24.

13. Vengudusamy B, Green JH, Lamb GD, Spikes HA. Durability of ZDDP Tribofilms Formed in DLC/DLC Contacts. Tribol Lett. 2013 Sep;51(3):469–78.

14. Vengudusamy B, Green JH, Lamb GD, Spikes HA. Tribological properties of tribofilms formed from ZDDP in DLC/DLC and DLC/steel contacts. Tribology International. 2011 Feb;44(2):165–74.

15. Sheasby JS, Caughlin TA, Habeeb JJ. Observation of the antiwear activity of zinc dialkyldithiophosphate additives. Wear. 1991 Oct;150(1–2):247–57.

16. Bird RJ, Galvin GD. The application of photoelectron spectroscopy to the study of e. p. films on lubricated surfaces. Wear. 1976 Apr;37(1):143–67.

17. Bell JC, Delargy KM, Seeney AM. Paper IX (ii) The Removal of Substrate Material through Thick Zinc Dithiophosphate Anti-Wear Films. Tribology and Interface Engineering Series. 1992;21:387–96.

18. Georges JM, Martin JM, Mathia T, Kapsa Ph, Meille G, Montes H. Mechanism of boundary lubrication with zinc dithiophosphate. Wear. 1979 Mar;53(1):9–34.

19. API Engine Oil Classifications: Service Fill Oils for Gasoline, Light-Duty Diesel And Heavy-Duty Diesel Engines [Internet]. Infineum; 2020. Available from: https://www.infineum.com/media/w5kpot0y/api-engine-oil-classifications-brochure2.pdf

20. Rensselar JV. Special report: The tribology of electric vehicles. Tribology and lubrication technology. 2019 Jan;75(34).

21. Chen Y, Jha S, Raut A, Zhang W, Liang H. Performance Characteristics of Lubricants in Electric and Hybrid Vehicles: A Review of Current and Future Needs. Front Mech Eng. 2020 Oct 14;6:571464.

22. Khare HS, Lahouij I, Jackson A, Feng G, Chen Z, Cooper GD, et al. Nanoscale Generation of Robust Solid Films from Liquid-Dispersed Nanoparticles via in Situ Atomic Force Microscopy: Growth Kinetics and Nanomechanical Properties. ACS Appl Mater Interfaces. 2018 Nov 21;10(46):40335–47.

23. Elinski MB, LaMascus P, Zheng L, Jackson A, Wiacek RJ, Carpick RW. Cooperativity Between Zirconium Dioxide Nanoparticles and Extreme Pressure Additives in Forming Protective Tribofilms: Toward Enabling Low Viscosity Lubricants. Tribol Lett. 2020 Dec;68(4):107.

24. Lahouij I, Gould B, Demas N, Greco A, Chen Z, Cooper GD, et al. Inhibition of Micro-pitting by Tribofilm-Forming ZrO2 Nanocrystal Lubricant Additives: A Micro-pitting Rig and Transmission Electron Microscope Study. Tribol Lett. 2022 Mar;70(1):13.

25. Kato H, Komai K. Tribofilm formation and mild wear by tribo-sintering of nanometer-sized oxide particles on rubbing steel surfaces. Wear. 2007 Jan;262(1–2):36–41.

26. Dorgham A, Parsaeian P, Azam A, Wang C, Morina A, Neville A. Single-asperity study of the reaction kinetics of P-based triboreactive films. Tribology International. 2019 May;133:288–96.

27. Gosvami NN, Ma J, Carpick RW. An In Situ Method for Simultaneous Friction Measurements and Imaging of Interfacial Tribochemical Film Growth in Lubricated Contacts. Tribol Lett. 2018 Dec;66(4):154.

28. Zhang J, Ewen JP, Ueda M, Wong JSS, Spikes HA. Mechanochemistry of Zinc Dialkyldithiophosphate on Steel Surfaces under Elastohydrodynamic Lubrication Conditions. ACS Appl Mater Interfaces. 2020 Feb 5;12(5):6662–76.

29. Spikes H. Stress-augmented thermal activation: Tribology feels the force. Friction. 2018 Mar;6(1):1–31.

30. Mosey NJ, Woo TK, Müser MH. Mechanism of wear inhibition by ZDDP lubricant additives - Insights from molecular scale simulations. American Chemical Society. 2005;4.

31. Mosey NJ. Molecular Mechanisms for the Functionality of Lubricant Additives. Science. 2005 Mar 11;307(5715):1612–5.

32. Mosey NJ, Woo TK, Kasrai M, Norton PR, Bancroft GM, Müser MH. Interpretation of experiments on ZDDP anti-wear films through pressure-induced cross-linking. Tribol Lett. 2006 Nov 13;24(2):105–14.

33. Mosey NJ, Woo TK, Müser MH. Energy dissipation via quantum chemical hysteresis during high-pressure compression: A first-principles molecular dynamics study of phosphates. Phys Rev B. 2005 Aug 25;72(5):054124.

34. Righi MC, Loehlé S, De Barros Bouchet MI, Mambingo-Doumbe S, Martin JM. A comparative study on the functionality of S- and P-based lubricant additives by combined first principles and experimental analysis. RSC Adv. 2016;6(53):47753–60.

35. Bec S, Tonck A, Georges JM, Coy RC, Bell JC, Roper GW. Relationship between mechanical properties and structures of zinc dithiophosphate anti–wear films. Proc R Soc Lond A. 1999 Dec 8;455(1992):4181–203.

36. Martin JM. Antiwear mechanisms of zinc dithiophosphate: a chemical hardness approach. Tribology Letters. 1999;6:1–8.

37. Dawczyk J, Morgan N, Russo J, Spikes H. Film Thickness and Friction of ZDDP Tribofilms. Tribol Lett. 2019 Jun;67(2):34.

38. Stevie FA, Sedlacek L, Babor P, Jiruse J, Principe E, Klosova K. FIB-SIMS quantification using TOF-SIMS with Arand Xe plasma sources. Surface and Interface Analysis. 2014;46:285–7.

39. Wilson RG, Stevie FA, Magee CW. Secondary Ion Mass Spectrometry: A Practical Handbook for Depth Profiling and Bulk Impurity Analysis. 1st edition. New York: Wiley-Interscience; 1989. 384 p.

40. Willermet PA, Carter RO, Boulos EN. Lubricant-derived tribochemical films—An infra-red spectroscopic study. Tribology International. 1992 Jan;25(6):371–80.

41. Bell JC, Coy RC, Spikes HA. Cryogenic Studies of Zinc Dialkyl Dithiophosphate Anti-wear Films. Proc Japanese International Tribology Conference. 1990;505.

42. Bell JC, Delargy KM. The composition and structure of model zinc dialkyldithiophosphate antiwear films. Proceeding of the 6th International Congress on Tribology. 1993;2:328–32.

43. Minfray C, Martin JM, Barros MID, Mogne TL, Kersting R, Hagenhoff B. Chemistry of ZDDP Tribofilm by ToF-SIMS. Tribology Letters. 2004 Oct;17(3):351–7.

44. Bell G. Models for the specific adhesion of cells to cells. Science. 1978 May 12;200(4342):618–27.

45. Lomakina E, Waugh RE. Bond formation during cell compression. In: Principles of Cellular Engineering. Elsevier; 2006. p. 105–22.

46. Chen B, Hoffmann R, Cammi R. The Effect of Pressure on Organic Reactions in Fluids—a New Theoretical Perspective. Angew Chem Int Ed. 2017 Sep 4;56(37):11126–42.

47. Ward IM. Review: The yield behaviour of polymers. Journal of materials science. 1971;6(11):1397–417.

48. Yamaguchi ES, Ryason PR, Labrador EQ. Inelastic Electron tunneling spectra of neutral and basic ZDDP on Native Aluminum oxide surfaces. Tribology transactions. 1995;38(2).

49. Ivanov AV, Antzutkin ON, Larsson AC, Kritikos M, Forsling W. Polycrystalline and surface O,O′-dialkyldithiophosphate zinc(II) complexes: preparation, 31P CP/MAS NMR and single-crystal X-ray diffraction studies. Inorganica Chimica Acta. 2001 Apr;315(1):26–35.

50. Jones RB, Coy RC. The Chemistry of the Thermal Degradation of Zinc Dialkyldithiophosphate Additives. ASLE preprints. 1979;1–7.

51. Stachowiak GW, Batchelor AW. Physical Properties of Lubricants. In: Engineering Tribology. Elsevier; 2014. p. 11–50.

52. Barus C. Isothermals, isopiestics and isometrics relative to viscosity. Am J Sci. 1893 Feb 1;s3-45(266):87.

53. Bair S. The unresolved definition of the pressure-viscosity coefficient. Sci Rep. 2022 Dec;12(1):3422.

54. Martin JM, Grossiord C, Mogne TL, Bec S, Tonck A. The two-layer structure of Zndtp tribofilms Part I: AES, XPS and XANES analyses. Tribology International. 2001;8.

55. Martin JM, Onodera T, Minfray C, Dassenoy F, Miyamoto A. The origin of anti-wear chemistry of ZDDP. Faraday Discuss. 2012;156:311.